# Accepted Manuscript

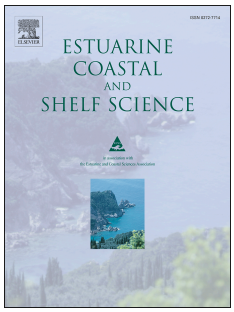


Contrasting structural patterns of the mesozooplankton community result from the development of a frontal system in San José Gulf, Patagonia

Rodrigo D. Hernández-Moresino, Rosana Di Mauro, Augusto C. Crespi-Abril, Gabriela L. Villanueva-Gomila, Jesus C. Compaire, Pedro J. Barón

PII: S0272-7714(17)30325-6

DOI: 10.1016/j.ecss.2017.05.012

Reference: YECSS 5481

To appear in: *Estuarine, Coastal and Shelf Science*

Received Date: 23 March 2017

Accepted Date: 15 May 2017

Please cite this article as: Hernández-Moresino, R.D., Di Mauro, R., Crespi-Abril, A.C., Villanueva-Gomila, G.L., Compaire, J.C., Barón, P.J., Contrasting structural patterns of the mesozooplankton community result from the development of a frontal system in San José Gulf, Patagonia, *Estuarine, Coastal and Shelf Science* (2017), doi: 10.1016/j.ecss.2017.05.012.

# Contrasting structural patterns of the mesozooplankton community result from the development of a frontal system in San José Gulf, Patagonia

**Rodrigo D. Hernández-Moresino[a,*], Rosana Di Mauro[b], Augusto C. Crespi-Abril[a,c,e], Gabriela L. Villanueva-Gomila[a], Jesus C. Compaire[d] and Pedro J. Barón[a,e]**

[a] Centro para el Estudio de Sistemas Marinos, Consejo Nacional de Investigaciones Científicas y Técnicas (CESIMAR-CONICET), Puerto Madryn, Chubut, Argentina.

[b] Department of Oceanography and Coastal Science, Louisiana State University, Baton Rouge, LA, USA.

[c] Universidad Nacional del Comahue, San Antonio Oeste, Río Negro, Argentina.

[d] Departamento de Biología, Facultad de Ciencias del Mar y Ambientales, Universidad de Cádiz, Cádiz, Spain.

[e] Facultad de Ciencias Naturales, Universidad Nacional de la Patagonia San Juan Bosco, Puerto Madryn, Chubut, Argentina.

* Corresponding author at: Centro para el Estudio de Sistemas Marinos, Consejo Nacional de Investigaciones Científicas y Técnicas (CESIMAR-CONICET), Boulevard Brown 2915, Puerto Madryn (U9120ACD), Chubut, Argentina. Tel: +54 280 4883184. E-mail: *rodrigo@cenpat-conicet.gob.ar*

## Abstract

The structural patterns of the mesozooplankton community of San José Gulf (SJG), a one of a kind semi-enclosed basin located in the northern margin of the Valdés Peninsula (Argentine Patagonia), were studied by means of semi-automatic image analysis. Samples were obtained bimonthly during the warm season (October 2012-April 2013) at stations distributed on a regular grid. Cluster analyses outlined two spatially consistent groups of stations showing similar patterns when based on physical (SST, Chl-a, and bottom depth) and

community structure (abundance, biomass, and slope of the size spectra) descriptors, each broadly distributed on one of two previously described hydrographic domains formed by the interaction of tidal circulation, coastal morphology, bottom topography, and seasonal vertical stratification. Examination of the slope of the mesozooplankton size spectra revealed that the stratified waters of the East Domain sustain higher proportions of small organisms and higher biomass, suggesting potentially low trophic transfer efficiency compared to its vertically-mixed West counterpart. Three-clustering analyses resulted in still spatially consistent groups of stations when based on the community descriptors, revealing the existence of a transition zone, presumably resulting from intermediate hydrodynamic conditions. Principal component analysis revealed that biomass of cladocerans modulates the size spectra and is related with distances from sampling stations to SJG´s mouth. Overall, a consistent spatial correlate was found between physical conditions of water masses and the structure of the mesozooplancton community contained within.

Keywords: mesozooplankton; community structure; hydrodynamic conditions; San José Gulf; ZooImage.

## 1. Introduction

Oceans are characterized by a marked spatial variation in productivity (Platt and Harrison, 1985; Lewis, 2002). Many oceanic environments have low productivity due to poor availability of nutrients in the surface layers even in the presence of high levels of photosynthetic available radiation. In contrast, others are characterized by high productivity promoted by hydrodynamic processes (i.e., upwelling, thermal stratification, and currents) that produce vertical mixture of water masses and vertical pumping of nutrient-rich waters into the photic zone (Mann and Lazier, 1991; Belkin et al., 2009). Some of these processes are responsible for the development of oceanographic discontinuities known as frontal systems. A frontal system can be thought of as an encounter of water masses with different physical properties (e.g., temperature, density) in which circulation patterns generate a convergence with a sharp transition, even in the presence of diffusive effects (Largier, 1993), occurring at several spatial and temporal scales (Acha et al., 2015). These systems are of biological relevance in oceanic and coastal environments because they frequently promote high primary productivity sustaining the trophic networks, and thus organisms with value for human consumption (Mackenzie, 2002; Crespi-Abril, 2012; Acha et al., 2015).

San José Gulf (SJG) is a shallow, semi-enclosed and highly productive basin located in the northern coast of Argentine Patagonia. Its northwestern margin presents a narrow mouth that connects with the much larger and deeper San Matías Gulf (SMG) (Fig. 1A). Tidal circulation has a major role on the hydrodynamic structure of SJG. During each semi-diurnal tidal cycle, up to 15% of its total volume flows in and out through its mouth (Rivas, 1990). Since this process is longitudinally asymmetrical, a strong year-round semilunar tidal circulation in the western portion produces a homogeneous structure of the water column,

while the eastern side of the gulf is less affected allowing spring-summer stratification (Amoroso et al., 2011; Crespi-Abril et al., 2014). The result is the formation of a frontal system between a west (WD) and east (ED) hydrographic domains (Gagliardini et al., 2004; Amoroso and Gagliardini, 2010). The complexity of the system is further enhanced by the arrival of cold waters from the coastal, vertically mixed side of the tidal front developed off Valdés Peninsula (Amoroso and Gagliardini, 2010; Pisoni et al., 2015). These water masses generate a highly productive area during spring and summer due to the surface nutrient enrichment produced by vertical mixing (Carreto et al., 1986). Therefore, SJG provides a unique scenario to study the mesozooplankton community structuring in response to small mesoscale contrasting physical conditions.

Many studies have shown that distinct hydrographic conditions prevailing in different domains of a frontal system can determine dissimilar patterns in size spectra, biomass, and species composition of zooplankton communities (Sabatini and Martos, 2002; Alcaraz et al., 2007; Manríquez et al., 2009). Scientific interest in this phenomenon is related to its ecological significance and its consequences for fisheries management. Among other aspects, frontal systems provide a good scenario to test hypothesis about the heterogeneous distribution patterns of planktonic species and the formation of different trophic pathways in neighboring areas (Mauna et al., 2008; Alemany et al., 2009, 2014).

In marine ecosystems the size spectra of pelagic communities has long been considered an important topic since the initial work of Sheldon et al. in 1972 (Platt and Denman, 1977, Quinones et al., 2003). However, the analysis of zooplankton size spectra is not an easy task since it requires the measurement of many organisms in many samples. In this regard, semi-automatic analysis based on digitized images, developed in the last decades, has become a widely popular and highly valuable tool to accelerate sample

processing, providing identification (variable taxonomic resolution), quantification, and measurements of zooplankton (Benfield et al., 2007; Bell and Hopcroft, 2008; Fernandes et al., 2009; Gorsky et al., 2010). The analysis of size spectra (i.e., the distribution of abundance or volume relative to the size of the organisms) is particularly useful to study the plankton community structure. Size-based indices have been widely used as an alternative or complementary approach to describe marine communities (Jennings et al., 2002; Shin et al., 2005; Krupica et al., 2012). One example of such application is the normalized biomass size spectrum (NBSS) theory (Kerr and Dickie, 2001). With a solid theoretical and empirical foundation, the size spectra can reveal patterns and explain variation in aquatic communities that are neither apparent nor conceivable from conventional taxonomic approaches.

Quantitative empirical analyses of plankton size spectra are usually based on the parameters generated by a straight line fitted to the size spectrum (linear regression type I). In particular, the slope of the size spectra has been widely used as a metric of size structure (Zhou, 2006 and references therein): the steeper the slope, the higher the contribution of small organisms to the bulk biomass of the community. Other applications of this theory associate the parameters from the linear regression with biomass production rates, energy transfer efficiencies and predator–prey interactions at regional and global scales (Shin et al., 2005).

A previous analysis of monthly mesozooplankton samples collected on a transect across the SJG frontal system has shown that stations from the vertically-mixed WD were dominated by larger zooplankton (mainly copepods) compared to those from the vertically stratified ED, in which cladocerans and small copepod species accounted for most of the abundance (Hernández-Moresino et al., 2014). Although that study revealed that the structure of the mesozooplankton community differed between stations along a transect crossing the

116 frontal system, it did not attempt to identify the hydrographic drivers modeling this difference,
117 neither it accounted for its variability throughout the entire gulf extension. In view of these
118 limitations, this study aims to test if contrasting hydrodynamic conditions prevailing in both
119 domains of the frontal system of SJG are reflected by the mesozooplankton community
120 structure.
121
122
123 **2. Materials and methods**
124
125 *2.1. Zooplankton sampling*
126 Zooplankton samples were collected with a Hensen net (0.7-m diameter and 295-µm
127 mesh) by performing near-bottom-to-surface oblique tows at ~ 1 m $s^{-1}$, using a mechanical
128 flowmeter mounted at the mouth of the net to measure the filtered volume (General Oceanics,
129 model R 2030). The sampling design consisted of a fixed grid of 19 stations distributed within
130 SJG (10 in the WD, 9 in the ED) at the time of development of the frontal system, starting in
131 October 2012 and ending in April 2013. Rough weather conditions or presence of whales
132 interrupted the sampling in one station in 2012 and four stations during 2013. In total, 71
133 zooplankton samples were obtained at the end of the survey. Large jellyfish were removed
134 from the samples before preservation in 5% formalin for subsequent analysis.
135

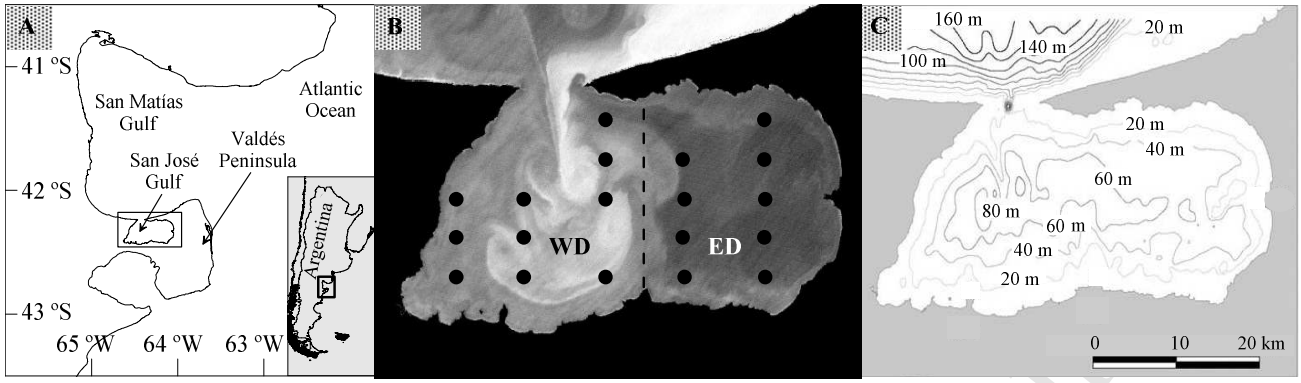


**Figure 1.** (**A**) Location of the San José Gulf. (**B**) Landsat image illustrating the distribution of suspended sediments (lighter tones correspond to higher sediment concentration). Image provided by R. A. Amoroso and D. A. Gagliardini. Black circles in B indicate the location of sampling stations. The broken line indicates the approximate location of the frontal system (Amoroso et al., 2011). WD: West Domain. ED: East Domain. (**C**) Bottom topography (SHN, 2000).

*2.2. Image processing and analysis*

Taxonomic identification and quantification was conducted by semi-automatic analysis of digital images with ZooImage software v1.2 (http://zooimage-team.software.informer.com/). Depending on the abundance of individuals in the samples, aliquots of 2 to 8% of the total volume, were stained with Bengal Rose for 24 h to enhance contrast, and photographed with a Nikon D3100 14.2 Mp camera mounted in a mechanical arm to fix the distance between the camera and the sampling cell. For calibration purposes a microgradiated ruler was photographed and measured using ImageJ, obtaining a pixel size equivalent to 0.018 mm. To predict zooplankton identification, a training set was built by manually sorting objects from samples taken from randomly chosen sampling stations covering all sampling months into user-defined taxonomic categories: Copepoda, Cladocera, Decapoda (decapod larvae), Chaetognatha, Malacostraca other (excluding decapod larvae), Appendicularia, Fish (fish

156 larvae), Elongated eggs, and Rounded eggs. Three non-biological categories (bubbles,
157 scratch and fibers, and shadows) were added to the training set to reduce contamination. The
158 total number of objects included in the training set was about 4000.

159 The Random Forest algorithm was selected for machine learning, on account that it is
160 one of the most accurate in the automatized processing of samples with ZooImage (Bell and
161 Hopcroft, 2008; Fernandes et al., 2009; Irigoien et al., 2009). The performance of the
162 automatic classification was evaluated by 10-fold cross-validation to identify misclassifications
163 between the categories, and its accuracy was improved up to a maximum of 90.6%. As a
164 result, a confusion matrix was obtained that not only allowed the identification of the wrongly
165 classified objects but also of categories from which these originate (Table 1). In addition, to
166 obtain more accurate estimations of abundance (ind. $m^{-3}$), predictions of each category were
167 corrected using coefficients calculated from the confusion matrix (CC = visual inspection /
168 ZooImage classification) (Table 1).

169

170 **Table 1.** Confusion matrix obtained from the training set. Numbers in the diagonal (in
171 grey) represent the correct classification of objects (true positives), while those outside
172 correspond to misclassified objects (false positives). CC denotes the correction coefficient
173 used to generate more accurate estimations of abundance.

**CONFUSION MATRIX**

| User classification in training set | General Accuracy (%) 90.65 | ZooImage classification prediction | | | | | | | | | | | CC |
|---|---|---|---|---|---|---|---|---|---|---|---|---|---|
| | | 1 | 2 | 3 | 4 | 5 | 6 | 7 | 8 | 9 | 10 | 11 | |
| | Appendicularia (1) | 24 | 0 | 2 | 0 | 1 | 2 | 0 | 0 | 0 | 2 | 0 | 1.42 |
| | Bubbles (2) | 0 | 236 | 0 | 0 | 0 | 0 | 0 | 0 | 0 | 0 | 14 | 1.01 |
| | Chaetognatha (3) | 1 | 0 | 132 | 0 | 0 | 2 | 0 | 0 | 0 | 0 | 0 | 1.10 |
| | Cladocera (4) | 0 | 1 | 0 | 629 | 3 | 19 | 2 | 3 | 13 | 0 | 4 | 0.97 |
| | Copepoda (5) | 4 | 0 | 7 | 2 | 1227 | 90 | 0 | 0 | 20 | 0 | 0 | 0.96 |
| | Decapoda (6) | 14 | 1 | 8 | 4 | 64 | 703 | 0 | 0 | 27 | 0 | 2 | 1.02 |
| | Egg-ellongated (7) | 0 | 0 | 0 | 2 | 0 | 1 | 211 | 1 | 0 | 0 | 0 | 0.99 |
| | Egg-round (8) | 0 | 0 | 0 | 2 | 0 | 0 | 0 | 133 | 0 | 0 | 0 | 1.02 |
| | Malacostraca other (9) | 0 | 0 | 0 | 14 | 1 | 19 | 0 | 0 | 141 | 0 | 0 | 1.15 |
| | Scrachs-Fibers (10) | 1 | 0 | 0 | 0 | 0 | 0 | 0 | 0 | 0 | 102 | 9 | 0.98 |
| | Shadowa (11) | 0 | 15 | 0 | 1 | 0 | 0 | 0 | 1 | 0 | 6 | 193 | 1.03 |
| | **Total** | 44 | 253 | 149 | 654 | 1296 | 836 | 213 | 138 | 201 | 110 | 222 | |
| | **Accuracy (%)** | 54.5 | 93.3 | 88.6 | 96.2 | 94.7 | 84.1 | 99.1 | 96.4 | 70.1 | 92.7 | 86.9 | |

174

175

176 ZooImage also provided information on basic body size parameters such as length
177 (i.e., major axis of the best fitting ellipse), and width (i.e., minor axis), that can be used to
178 calculate biovolume size spectra. The individual ellipsoidal biovolume (*EBv*) for each
179 zooplankter was estimated using the equation of volume for a prolate ellipsoid:

180

$$EBv = \frac{4}{3} * \pi * \left(\frac{´Major\ axis}{2}\right) * \left(\frac{´Minor\ axis}{2}\right)^2$$

181

182 Given that biovolume should be a function of both the projected size and shape, and not only
183 of the projected size, the more realistic ellipsoidal biovolume model was chosen over the
184 spherical one based on the equivalent circular diameter (*ECD*) automatically provided by
185 ZooImage (Vandromme et al., 2012).

186

187 *2.3. Zooplankton community descriptors*

188 Three descriptors were used to characterize the zooplankton community: Abundance,
189 Slope of the size spectra, and Biomass. The first was estimated as the number of individuals

per unit of filtered volume (ind. $m^{-3}$), and was determined and standardized based on the flowmeter data.

Size spectra were computed by sorting the ellipsoidal body volume into size classes. The width of each size class was doubled with respect to the previous one following a geometric $2^{nd}$ series arrangement (Sheldon et al., 1972). The lowest limit of the first size class corresponded to the biovolume of the smallest organism that our net was able to retain, ~0.01 $mm^3$, while the largest size class contained organisms up to 1.31 x $10^3$ $mm^3$, making up a total of 18 classes. Biovolume values below the minimum were treated as contamination (i.e. fibers), and discarded from the data set. Spectra were normalized by dividing the total *EBv* of each size class ($mm^3$ $m^{-3}$) by its width ($mm^3$). Zero values in the spectra were treated as empty size classes and not included in the regression analysis. The spectra obtained by this procedure are termed Normalized Biovolume Size Spectra (*NBSS*) (Platt and Denman, 1977), hereafter referred to as size spectra.

The slope (*b*) of the size spectrum was calculated by fitting a linear regression (simple Model I regression) to the $\log_{10}$-$\log_{10}$ representation of the size spectra. When calculating the size spectra, underestimation of the smaller size classes may occur due to the size of the mesh used to collect the sample. To avoid this bias, we determined the mode of the entire biovolume spectrum (which corresponded to the $5^{th}$ size class, ~ 0.24 $mm^3$ nominal size), and values smaller than this lower limit were excluded to calculate the spectrum indices. Linear regressions showing significant slopes (Student´s t-test, $P < 0.01$) were included in further analysis, and Pearson's correlation coefficients (ρ from 0.88 to 0.99) were calculated for all of them.

The biomass of a given mesozooplankter was calculated using the regression equations from the relationship between individual dry mass and body area reported for

subtropical and Antarctic organisms (Hernández-León and Montero, 2006; Lehette and Hernández-León, 2009):

$$DW = 43.38 * S^{1.54},$$

where *DW* is the dry weight and *S* is body area in $mm^2$.

For appendicularians, ZooImage tends to overestimate the body area by contemplating the size of the entire silhouette, so the general equation was applied only using the trunk length, leaving out the tail. To make this correction, we calculated the trunk area ($mm^2$) from 10 randomly chosen individuals using ImageJ tools, and applied a correction coefficient of 0.31 to the area estimated automatically.

Lastly, given that the fitting equation for chaetognaths was very different to that of the general mesozooplankton, we used a special equation for biomass estimation in this group (Lehette and Hernández-León, 2009):

$$DW = 23.45 * S^{1.19}$$

*2.4. Physical descriptors*

Temporal and spatial variation of sea surface temperature (SST) and chlorophyll a concentrations (Chl-a) were obtained using Moderate-resolution Imaging Spectrometer or MODIS Aqua level 3 satellite imagery with 4-km resolution. MODIS was chosen because it is readily available (http://oceancolor.gsfc.nasa.gov/), and because it has a multispectral sensor. The orbit is sun-synchronous, meaning that the satellite always passes over a particular part of the Earth at about the same local time each day. Since the cloud cover that usually forms

over the study area, data acquired for the sampling stations in a daily or even weekly basis had too many gaps. Thus monthly-average data were selected.

The depth of each sampling station corresponded to bottom depth in meters and was obtained directly from the echo sounder mounted in the ship. Distance from each sampling station to the center of SJG´s mouth was calculated using the Google Earth software (https://earth.google.com/).

Temperature-depth (TD) profiles were obtained during each zooplankton tow using a bathythermograph with a data logger attached to the net mouth (more details in Crespi-Abril et. al., 2014). Temperature and depth data were not available in December.Velocity of horizontal tidal circulation ($\mu$) at each sampling event was calculated using the equation developed for shallow water tidal currents (Knauss, 1978):

$$\mu = a * \sqrt{\frac{g}{H}} * sin(\omega * t)$$

with "*a*" being the tidal amplitude, "*g*" the gravity acceleration constant, "*H*" the depth in time t (bottom-surface distance plus tidal height), "$\omega$" is the tidal period and "*t*" time of sampling. Tidal amplitude and tidal period data were estimated with the software WXTide32 2.6. It is important to note that surface tidal currents are rotary; that is, a water particle would follow the path of an ellipse during a complete tidal circle. Predicting the ratio of major and minor axes and direction of rotation requires detailed knowledge of the tidal wave itself (Knauss, 1978). Thus, estimations of μ were absolute-transformed ($|\mu|$) to discard potential errors in the estimation of the direction and sense of tidal currents.

*2.5. Data analysis*

Spatiotemporal descriptors of the mesozooplankton community (i.e., abundance, biomass, and slope of the size spectrum), and physical conditions of SJG (SST, Chl-a, and depth) were inspected separately by applying K-means cluster analysis, a data-mining technique which algorithm has been used in several community structure studies (Escribano and Hidalgo, 2000; Punchi-Manage et al., 2013; Vandromme et al., 2014; Harris et al., 2015). This algorithm is better than the traditional numerical simulation model because it is relatively simple to implement and allows partitioning data into subsets based on non-linear relationships between the characteristics of the ecosystem (Chang et al., 2012). To facilitate comparisons, the data was normalized (Mean = 0 and Standard deviation = 1). For evaluation of the system dynamics over the evolution of the frontal system, analyses were first conducted for each month's data, and then gathering all months together in order to find a general spatial pattern. In the first case only stations with data were included in the analysis, while in the second, mean-substitution of missing data (i.e., mean of all stations for a given month) was implemented to include all the sampling stations..

Environmental (i.e., physical) and spatial variables were incorporated in a Principal Component Analysis (PCA) to identify those that may have higher effects on biological descriptors of the mesozooplankton community structure. The analysis included Chl-a, SST, $|\mu|$, distance to the gulf´s mouth, and depth. In terms of biological descriptors, the analysis included the slope of the size spectra and the biomasses of the most relevant biological groups (>5% of the total biomass; i.e., Copepoda, Cladocera, Decapoda, and Chaetognatha). The slope of the size spectra and biomass of key taxa were added as biological variables for the analysis, while environmental and spatial variables were added as supplementary ones. In addition, months were considered as the grouping variable. A correlation matrix was used

283 to calculate eigenvectors and principal components (PCs). For component significance in
284 PCA, we used eigenvalues > 1 (Bandalos and Boehm-Kaufman, 2009).
285 Additional statistical analyses were performed using two-way ANOVA followed by
286 Tukey´s HDS test to discriminate the differences showed by the k-means cluster analysis.
287 When normality and homoscedasticity assumptions were not met, nonparametric two-way
288 Kruskal-Wallis test was used, followed by the Dunn post hoc test (Conover, 1999).
289

290 **3. Results**

291
292 The taxonomic composition of the SJG´s mesozooplankton community was dominated
293 by cladocerans, copepods, decapods, and chaetognaths (Table 2). The remaining taxonomic
294 groups showed low relative abundance and low relative contribution to total biomass (5.45%
295 total) (Table 2).
296
297 **Table 2.** Taxonomic composition of the mesozooplankton community in San José Gulf.
298 Abundance (ind $m^{-3}$) and Biomass (mg $m^{-3}$) represent average values of all samples. Eggs
299 incude elongated and rounded shapes.

| Taxonomic Categories | Abundance (ind $m^{-3}$) | Biomass (mg $m^{-3}$) | Abundance (%) | Biomass (%) |
|---|---|---|---|---|
| Copepoda | 157.60 | 2.45 | 27.43 | 45.63 |
| Decapoda | 18.44 | 1.46 | 3.21 | 27.22 |
| Cladocera | 362.40 | 0.82 | 63.07 | 15.14 |
| Chaetognatha | 4.03 | 0.35 | 0.70 | 6.56 |
| Malacostraca other | 10.70 | 0.13 | 1.86 | 2.42 |
| Eggs | 12.86 | 0.12 | 2.24 | 2.15 |
| Fish | 0.08 | 0.04 | 0.01 | 0.78 |

| | | | | |
|---|---|---|---|---|
| Appendicularia | 8.52 | 0.01 | 1.48 | 0.10 |

The representation of the spatiotemporal variation of the total mesozooplankton biomass in the entire gulf showed that most of the stations presented higher values at the beginning of spring (October) (Fig 2). The following months were characterized by localized peaks observed in the northeastern corner of the ED (December and April), and in stations near the coast, with distinctive maxima at the south-eastern corner (February, Fig. 2). The second mesozooplankton biomass peak of February matched with the major development of the thermocline in the ED (Fig. 3).

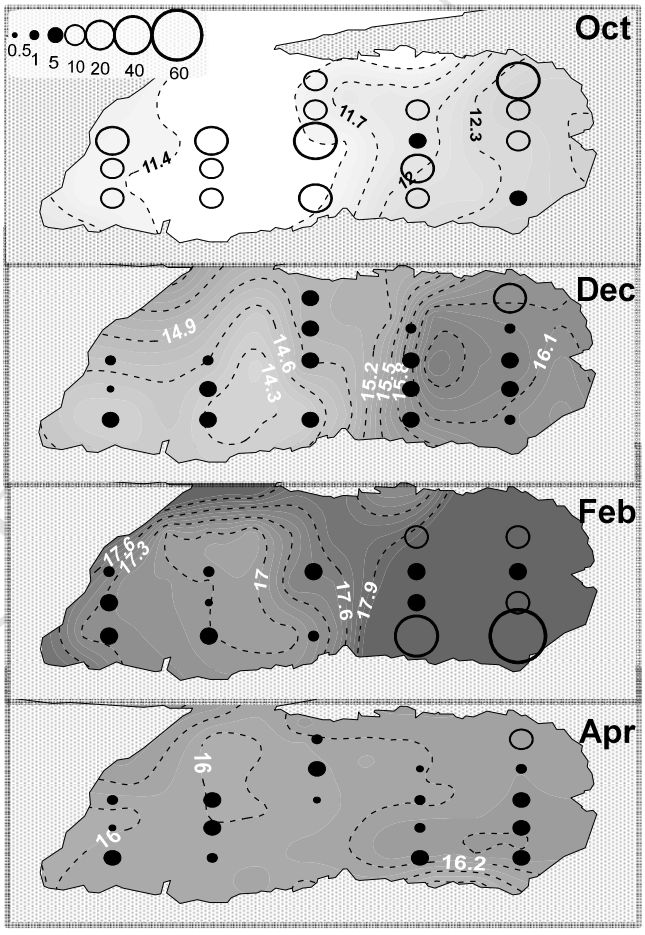

310 **Figure 2.** Spatiotemporal patterns of the total mesozooplankton biomass and SST.
311 Size circles refer to total biomass (mg $m^{-3}$), dashed lines represent SST isolines (in □C) and
312 darker tones indicate higher SST.

313

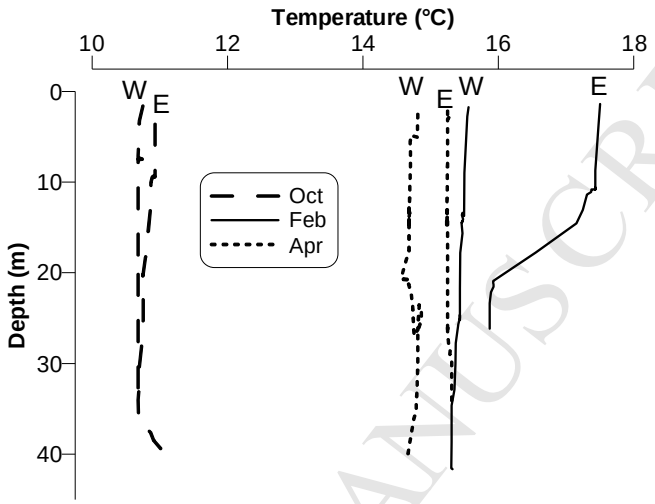


314

315 **Figure 3.** Representative vertical profiles of water temperature, taking two selected
316 sampling stations: one from the East Domain (E, station 4) and the other from the West
317 Domain (W, station 16).

318

319 The K-means exploratory analysis of physical descriptors (i.e., SST, Chl-a, and depth)
320 grouped the stations in two clusters that spatially corresponded with the hydrographic WD
321 and ED in February (i.e., when maximum stratification developed in the ED, Fig. 3) and when
322 cluster analysis was performed with all months together (Fig. 4A and B, respectively).
323 Contrarily, in October and December, when there was no stratification or it was just starting to
324 develop (Fig. 3), there was no clear-cut spatial correlation between eastern and western
325 stations and the ED and WD (Fig. 4A).

326 Similarly, analysis based on the community descriptors (i.e., abundance, biomass and
327 slope of the size spectra) grouped the stations in two clusters that spatially corresponded with

328 the hydrographic WD and ED only in February. Considering all months together the cluster of
329 stations from the West extended beyond the eastern boundary of the hydrographic WD, while
330 that from the East was reduced to only six stations (Fig. 4D). Community clustering in October
331 coincided to some extent with the hydrographic WD and ED, but those from December and
332 April showed scattered spatial patches not clearly associated with the hydrographic domains
333 (Fig. 4C).
334

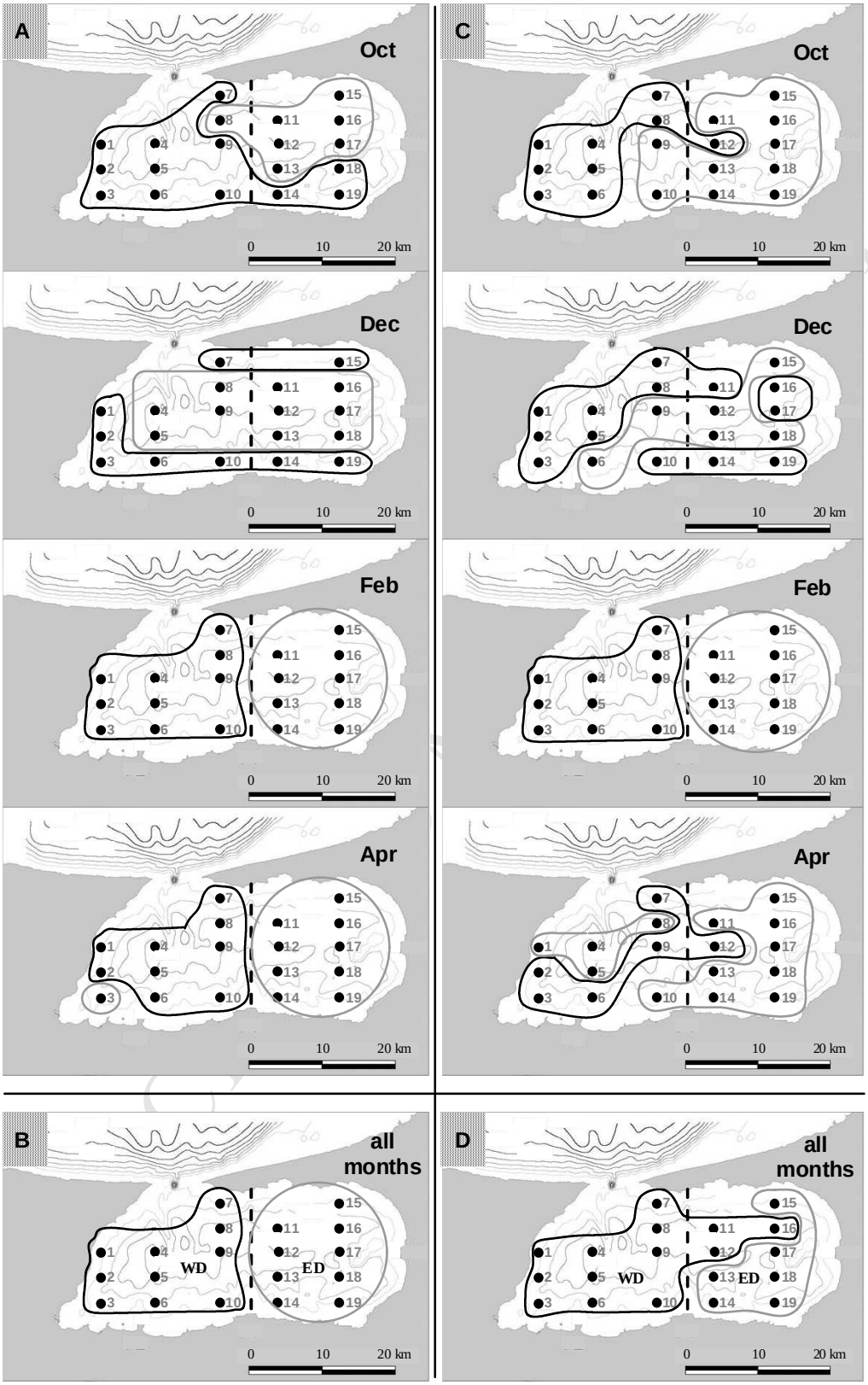
A
Oct
Dec
Feb
Apr
C
Oct
Dec
Feb
Apr
B
all months
WD
ED
D
all months
WD
ED
0
10
20 km

335

**Figure 4.** Groups of sampling stations based on two K-means clustering of physical and community descriptors. Left panel shows clusters based on physical descriptors for each month and for all months together (A and B, respectively). Right panel shows clusters based on community descriptors for each month and for all months together (C and D, respectively). The dashed line indicates the approximate location of the boundary between hydrographic WD and ED according to Amoroso et al. (2011).

Two-factor (month * cluster) Kruskal-Wallis tests revealed significant differences in SST ($H$ = 66.42, $P$ < 0.01) and Chl-a ($H$ = 50.41, $P$ < 0.01), but not in depth ($H$ = 0.78, $P$ = 0.99) between months and between clusters of stations. Dunn post-hoc tests revealed differences in SST between months, but not between clusters (Fig. 5). For Chl-a, between-cluster significant differences were observed only in October (Fig. 5). Lower Chl-a values were detected in both clusters in February and in the western one in October (Fig. 5). Both the west and east clusters presented increasing SST until February, after which this started to drop. In the stations from the east cluster, Chl-a concentration dropped as SST increased until February, rising thereafter in April along with the vanishing thermal stratification (Figs. 3 and 5). Contrarily, the WD presented no clear Chl-a variation pattern during the evolution of the frontal system.

The two-way ANOVA conducted for each of the three community descriptors showed significant differences in the interaction between months and clusters, both for abundance and biomass ($F_{(3,63)}$, $P$ < 0.01) (Fig. 5). However, no interaction was registered for the slope of the size spectra ($P$ = 0.06) (Fig. 5). The post hoc comparisons indicated a reduction in abundance from October to December in the western community cluster that persisted throughout the summer with a similar pattern for biomass (i.e., average biomass of 9.3 and

360 1.1 mg dw $m^{-3}$ in October and December respectively), but with a slight increase in February
361 (average biomass of 1.5 mg dw $m^{-3}$) (Fig. 5). For the eastern community cluster however, this
362 increase was more pronounced (average biomass of 10.9 mg dw $m^{-3}$) but not sustained over
363 time (Fig. 5). In regards to the slope of the size spectra, significant differences were found in
364 both main effects (months and clusters), values in the western community cluster being
365 higher (flatter slope) than in its eastern counterpart, with minima in October and maxima in
366 February (Fig 5).
367

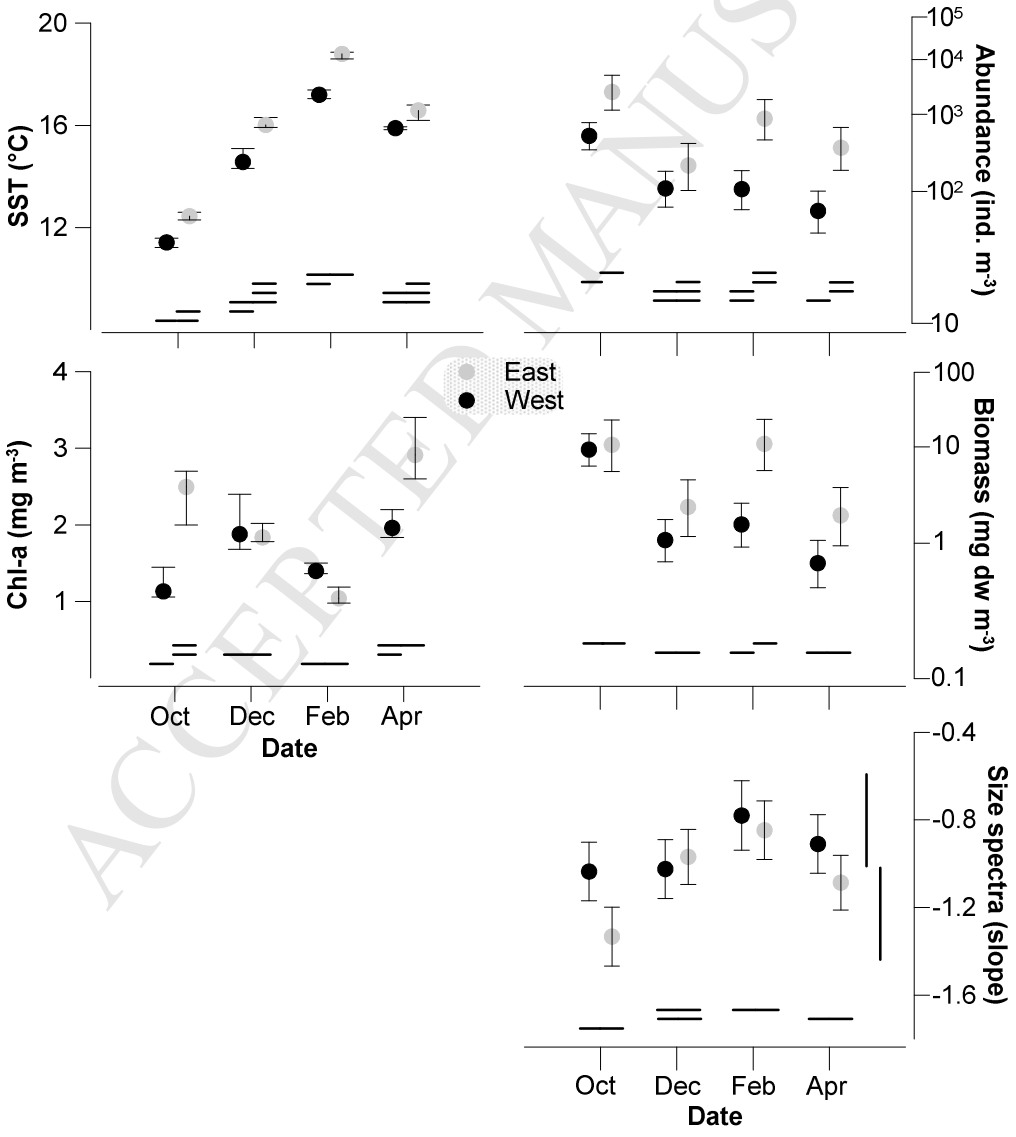


368

**Figure 5.** Temporal and spatial variability of physical and mesozooplankton community descriptors from San José Gulf. For physical descriptors, the two clusters of stations coincide with the hydrographic east and west domains (Amoroso et al., 2011). For community descriptors, the two clusters of stations correspond to month-aggregated data from the cluster analysis. For simplicity, in both cases clusters are referred to as from the West and East. Each horizontal bar in physical descriptor plots indicates a homogeneous group from Dunn´s test. Symbols and vertical whiskers denote median and inter-quartile range respectively. In community descriptor plots, each horizontal bar indicates a homogeneous group using Tukey´s HSD test, while symbols and vertical whiskers denote mean and 95% confidence intervals respectively. Vertical bars indicate differences between clusters.

Analysis of biomass variability for each taxon revealed that copepods mark the general pattern of the community, with the highest values in October in both clusters and a second peak only in the East in February (Fig. 6). On the other hand, decapods presented the highest biomass values in October and February, the first in the West and the second in the East (Fig. 6). Cladocerans showed a clear tendency to prevail in the East, with higher biomass values in October comparing to December and April (Fig. 6). Chaetognaths presented increasing biomass from October to February (Fig. 6). Remaining taxa only represented ca. 5% of the total biomass.

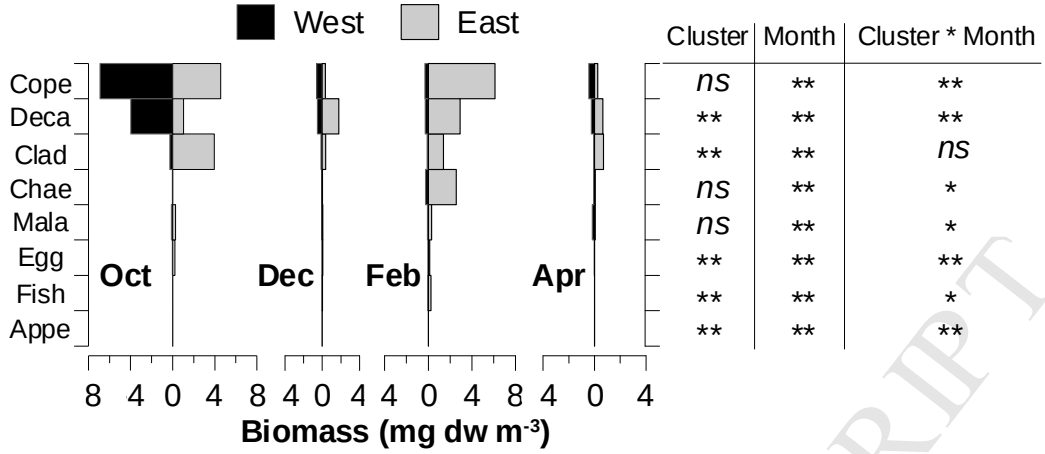


389

390 **Figure 6.** Mesozooplankton biomass per taxon and month in the western and eastern
391 communities (for simplicity West and East). Table indicates the signification of the two-way
392 ANOVA per each taxon. Symbols * and ** indicate $P < 0.05$ and $P < 0.01$ respectively, while
393 *ns* denote no significance. Cope: copepods, Deca: decapods, Clad: cladocerans, Chae:
394 chaetognaths, Mala: other malacostracans, Appe: appendicularians.

395

396 In order to further explore the effects of spatial and seasonal variation on both physical
397 (i.e., SST, Chl-a, and depth) and community descriptors (i.e., abundance, biomass, slope of
398 the size spectra), and in attempt to detect a transitional area between WD and ED, an
399 additional k-means cluster was set to classify sampling stations into three groups (Fig. 7).
400 Similarly to the previous cluster analysis, the stations on the west portion of the gulf
401 formed a group based on physical descriptors, while those from the ED split into two groups
402 of stations, one located in the deeper part of the ED, and the other, including three stations
403 placed closer to the coast (Fig. 7A). The two-factor (month * cluster) Kruskal-Wallis test for
404 SST was significant for the interaction ($H = 66.47$, $P < 0.01$). SST showed the same
405 increasing pattern until February as in the case of the two-cluster analysis (Fig. 5); however
406 no significant differences were detected between the three clusters in neither one month. For
407 Chl-a we also found significant differences in the month * cluster interaction ($H = 55.44$, $P <$

0.01), with higher values detected in October in the shallower portion of the ED compared to the WD and showing again the lowest values in February significantly different to those of April as in the case of the two cluster analysis. Depth only showed differences between clusters ($H$ = 20.18, P < 0.01); a cluster of shallow stations in the ED were separated from those of a deeper sector, while the stations in the WD presented intermediated values for this parameter.

Three-cluster analysis revealed that most stations facing the mouth of the gulf in its west portion shared similar values of their community descriptors, forming a still consistent namely “WD cluster”, as did the six stations located farther from the mouth on the southeast sector along with one at the northeast corner, hereafter the “ED cluster”. The third group, “transitional” between the two former, included four stations from the northeastern portion and two from the southwestern corner (Fig. 7B). Two-way ANOVAs revealed significant differences in the month * cluster interactions ($F_{(6,59)}$, $P < 0.01$ in all cases). Overall, the WD presented lower abundance and biomass, and higher slopes of the size spectra than de ED, while the transitional group evidenced intermediate values in some cases, as revealed by Tukey tests ($P < 0.01$). These groups are represented by the clusters in Figure 7B.

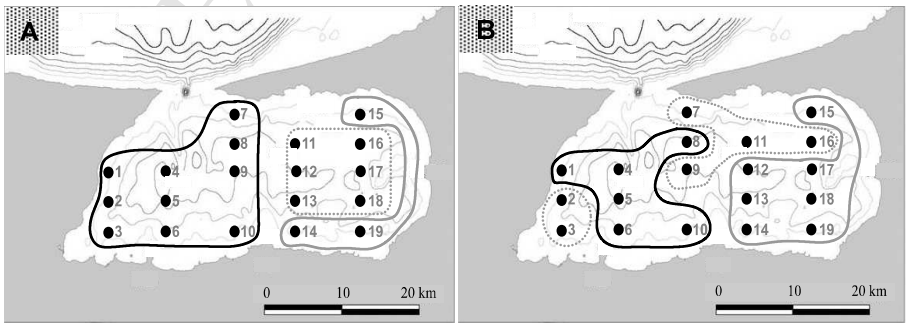


**Figure 7.** Clusters of stations based on physical (A) and community descriptors (B). Black and grey lines enclose stations belonging to the WD and ED, respectively, while

dashed grey lines identify deeper stations of the ED and transitional stations in terms of physical and community descriptor parameters, respectively.

In the PCA, PC1 and PC2 explained almost 80 % of the total variability of the biological community descriptors (Fig. 8). Biomass of cladocerans presented an inverse relationship with the slope of the size spectra and a direct one with the distance to the mouth that resulted significantly correlated (Pearson's ρ = 0.60 and 0.55, respectively) (Fig. 8). Another interesting finding was that biomasses of copepods and decapods (i.e., the taxa that contribute most to total biomass, Table 2) were positively related to $|\mu|$ (Pearson's ρ = 0.47, Fig. 8). Lastly, although chaetognath biomass was inversely related to Chl-a (Fig. 7), the relationship seem to be biased by the high biomass of chaetognaths occurring in a single month (i.e. February) when Chl-a concentrations were the lowest.

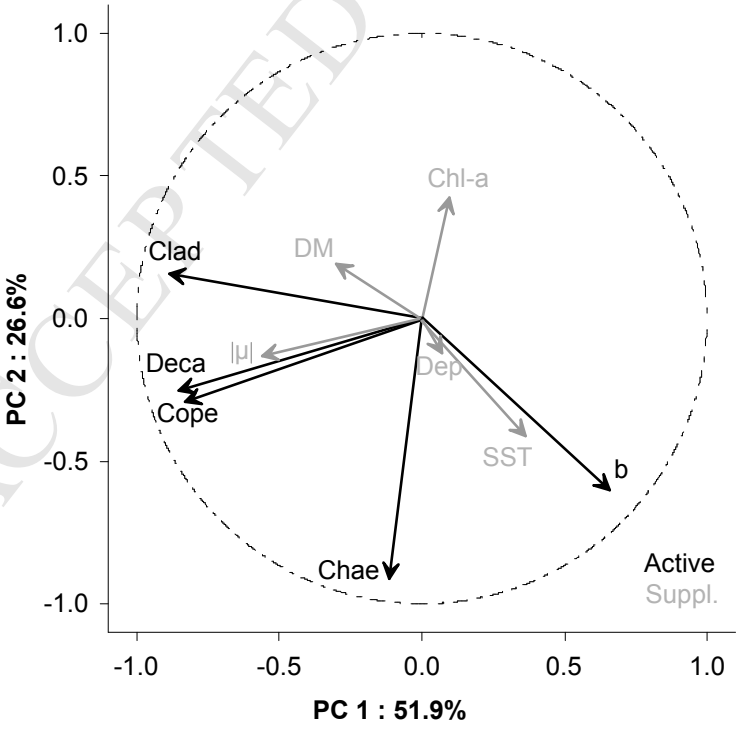

442 **Figure 8.** Results from PCA performed on community and physical descriptors of the
443 mesozooplankton community of SJG. Normalized eigenvectors 1 and 2 (78.5% of the total
444 variance). Circle of correlation (radius = 1) is displayed. Continuous black and grey arrows
445 represent active and supplementary variables, respectively. Cope: Copepod biomass; Deca:
446 Decapod biomass; Clad: Cladoceran biomass; Chae: Chaetognath biomass; b: slope of the
447 size spectra; SST: sea surface temperature; Chl-a: chlorophyll-a concentration; $|\mu|$: absolute
448 horizontal tidal circulation velocity; Dep: depth; DM: distance to the gulf´s mouth.
449
450 **4. Discussion**
451
452 The particular geomorphology of SJG (i.e, its semi-enclosed outline with an
453 asymmetrically located narrow mouth) is shared with just a few coastal accidents around the
454 world: Gulf of Coro (Venezuela), Bight of La Paz (Gulf of California, Mexico), Sherman Inlet
455 (Canada), Gulf of Riga (Baltic Sea, Latvia and Estonia), Pemba Bay (Mozambique), Ise and
456 Mutsu Bays (Japan), and Port Phillip Bay (Australia). All of them have microtidal regimes,
457 except for Pemba Bay, whose maximum tidal amplitude exceeds 5 m (Hoguane, 1999), being
458 still low compared to that of SJG (i.e, maxima exceeding 8 m; SHN, 2008). All of this makes
459 SJG one of a kind low-mesoscale (40 x 20 km) scenario to test the effects of hydrodynamics
460 on the mesozooplankton community structure.
461 Cluster analysis conducted in this study based on Chl-a SST and depth gives statistical
462 support to the characterization of two hydrographic domains in SJG postulated by Amoroso
463 and Gagliardini (2010). Patterns obtained from physical descriptor analyses were
464 straightforward when sampling stations were classified into two clusters based on all-month
465 data, as well as in February and April (Fig. 4A and B), while those from October were still

consistent with a differentiation of the west and east portions of the SJG. In contrast, December stations were grouped in a shallow and a deep cluster, probably because Chl-a values were relatively homogeneous through the gulf's extension.

As expected based on this robust physical differentiation and previous exploratory analysis conducted by Hernández-Moresino et al. (2014), a general spatial correlation was found between community structures of the mesozooplankton community and the hydrographic domains of SJG, except for three northern stations of the ED (11, 12 and 16; Fig. 4D) that shared the characteristics of those of the WD: flatter slope of size spectra (i.e., lower relative biovolume of small-sized mesozooplankters) and similar or lower abundance and biomass. When three-cluster analysis was conducted, it became evident that these stations belong to a transitional interphase between the WD and ED (Fig. 7B) whose spatial distribution cannot be explained based only on SST, depth, and Chl-a. Therefore, PCA was performed, showing a correlation between the velocity of horizontal tidal circulation ($|\mu|$) and the biomass of the most representative taxa (i.e., copepods and decapods) (Fig. 8). Nevertheless, it should be considered that $|\mu|$ is only a function of tidal amplitude, tidal moment, and bottom depth, and it does not take into account the effects of the particular geomorphology of SJG. Indeed, hydrodynamic modeling outputs reported by Moreira et al. (2011) indicated that velocity of horizontal tidal circulation in interior waters of the SJG is much weaker than near its shallow mouth (10-20 m deep, except for a narrow deep wedge at its center) (Fig 1.C). There, strong tidal currents occur as the tide wave passes through, pushing a jet of water into the gulf and generating highest vertical mixing in nearby stations (i.e., stations aligned with the mouth in the WD). Non-aligned stations located near the mouth, moderately sheltered from this circulation, should be less affected, while the more distant and sheltered stations of the ED should be almost unaffected. As flooding water enters through

490 the northwestern margin of the gulf, colder (and probably denser) mixed waters of the WD
491 could intrude to the ED below the warm surface stratum. Coriolis forces and bottom
492 topography (Fig 1.C) are propitious to channel these waters through the northern portion of
493 the ED. If that is the case, this sub-surface stream might be mixing and generating physical
494 conditions proper of the WD in the water column, poorly detectable by remote sensing of
495 surface conditions and could ultimately explain the spatial distribution of the three
496 mesozooplankton community clusters.

497 To interpret the structural differences in the mesozooplankton community between
498 mixed and stratified environments like those characterized in the SJG, one should keep in
499 mind that the pathways for flow of organic matter in pelagic food webs are, to a great extent,
500 determined by the food selectivity of the predators. Several criteria may be involved in food
501 selection, but prey selection of planktonic predators is primarily governed by size; hence prey
502 and predator size are positively correlated (Kiørboe, 2008). In frontal systems primary
503 producers show a direct response to nutrients and light. Turbulent and rich-nutrient
504 conditions, as may prevail in the WD of SJG, are generally dominated by large phytoplankton
505 cells (e.g. diatoms), while in vertically stratified and oligotrophic waters, as those from the ED
506 in February, small and often mobile phytoplankton (e.g. flagellates and cyanobacteria) should
507 be more frequent (Smayda, 1970). Larger cells sink faster than smaller cells, so they need
508 turbulent conditions to stay in the photic zone (Falkowski and Oliver, 2007). This would
509 promote the occurrence of larger mesozooplankton in turbulent conditions like those of the
510 WD, while stratification typical from the ED would benefit smaller herbivorous species (Le
511 Févre, 1986; Kiørboe, 1993). Furthermore, since phytoplankton must be continuously mixed
512 up and down, receiving enough light for growth only during the short moments it comes close
513 to the surface during the day, primary production must be accordingly lower than in the ED.

514 Thus, lower mesozooplankton biomass should be expected in the WD compared to that of the
515 ED, as was actually observed in February when maximum stratification occurred (Fig. 5). This
516 is in agreement with several studies where the main factor influencing structural changes in
517 the zooplankton community, that ultimately determines the high productivity areas, are
518 stratification and costal upwelling (Albaina and Irigoien, 2007; Alcaraz et al., 2007; Dur et al.,
519 2007; Lavaniegos et al., 2015).

520 Previous works showed that steeper spectrum slopes are related to a higher proportion
521 of small-sized herbivorous zooplankton with a role as retrievers of primary production by
522 grazing on small particles (Sprules and Munawar, 1986; Zhou, 2006; Zhou et al., 2009;
523 Marcolin et al., 2015). However, the size spectrum parameter was also related to ecosystem
524 productivity at other locations (e.g., Zhou et al., 2009; Basedow et al., 2010; Vandrome et al.,
525 2014), where steeper slopes of the size spectra relate to potentially low trophic transfer
526 efficiency. In this regard, cladocerans seemed to be the group with the highest influence in
527 shaping the community structure in the SJG due to their high relative abundance (63.5% of
528 the total), as reflected by the PCA (Fig. 8). In agreement to our results, previous studies
529 conducted in the frontal system off Valdés Peninsula have shown high abundances of
530 cladocerans in poorly mixed waters (Sabatini and Martos, 2002; Viñas et al., 2007, Derisio et
531 al., 2014), a more suitable environment for the rather low displacement velocities (10 to 50
532 times lower than those of copepods) that these organisms can reach (Allan, 1976). Also
533 markedly higher copepod biomass occurred in the ED in February, coinciding with the
534 stratification peak, in agreement with typical patterns observed across tidal fronts (Kiørboe,
535 2008), and particularly with their distribution in the neighboring Valdés Peninsula frontal
536 system in December (Spinelli et al., 2011; Derisio et al., 2014). In contrast, a more

537 homogeneous distribution of copepods was observed in both domains in October when the
538 front was not formed yet.

539 Concerning the temporal variation of the mesozooplankton biomass, one of the most
540 relevant patterns found in this work was the peak found in October (ca. 10 mg $m^{-3}$) and its
541 decrease throughout the summer. This was consistent with estimations made by Ramirez et
542 al. (1996) in the neighboring San Matías Gulf, where zooplankton biomass reached its
543 maximum in spring and its minimum in summer. In the ED however, a second biomass peak
544 was detected in February, which was also observed in the period 2011-2012 (Hernández-
545 Moresino et al., 2014). This event coincides with the lowest monthly Chl-a concentration
546 estimations, likely due to intensive foraging by zooplankton. However, this could also result
547 from inorganic nutrients exhaustion by phytoplankton in the euphotic zone, in which case
548 other factors apart from primary production must be involved in the determination of
549 secondary production (Albaina and Irigoien, 2004). One possible explanation for this pattern
550 could be that while only a classic herbivorous food web sustains the mesozooplankton
551 biomass in the WD, with larger organisms grazing on large phytoplankton cells, a combination
552 of that with a micro-heterotrophic pathway mediated by cladocerans, which are able to feed
553 on small particles including bacteria (Le Fèvre, 1986), could be giving additional support in
554 the ED. Other interesting temporal variation was the flattening of slope of the size spectra up
555 to February, affecting both domains similarly. This could result from a succession from
556 smaller to larger species or to individual growth throughout the season as discussed by
557 Hernández-Moresino et al. (2014). In this context, results from studies on coastal waters of
558 the Argentine Sea, near SJG, are in agreement with our observations on the temporal
559 mesozooplankton succession (Viñas et al., 2013): a cold winter-spring period characterized
560 by a dominant classical herbivore food web, in which large copepods associated with the

lowest temperature and the highest Chl-a concentration (October in SJG), and a warm summer period dominated by a microbial food web, in which filter-feeders such as small copepods, cladocerans and appendicularians predominate and the lowest Chl-a concentrations are recorded (February in SGJ).

Finally, since sampling methodology remained the same, our results can be contrasted with those obtained in the same season in 2011-2012 (Hernández-Moresino et al., 2014). Higher mesozooplankton abundances were recorded in that period as compared with those estimated for 2012-2013 (ca. 10.000 against 600 ind. $m^{-3}$, average values for each period respectively). In particular, relative abundances of dominant taxa in 2011-2012 was estimated to be 68.6% for copepods, and 16.3% for cladocerans, while in 2012-2013 such dominance pattern switched to 63.5% of cladocerans and 27.1% of copepods. This inter-annual variability, both in abundance and taxon dominance, could be associated to higher estimated Chl-a concentration in the first period (e.g., 6.0 mg $m^{-3}$ and 2.5 mg $m^{-3}$ average concentrations in the ED in October 2011 and 2012 respectively). Once more, this difference could result in two contrasting scenarios: one based on a classic heterotrophic pathway sustained by high Chl-a concentration and dominated by copepods (period 2011-2012) and the other based on a mixture of heterotrophic and micro-heterotrophic pathways occurring during less productive conditions, dominated by cladocerans (period 2012-2013).

**Contribution**

RD Hernández-Moresino participated in all stages of this work, R Di Mauro contributed with image analysis, interpretation of results and article preparation, AC Crespi-Abril with statistical analysis and its interpretation, GL Villanueva-Gomila was involved in

585 methodological decisions and field activities, JC Compaire was involved in zooplankton
586 preparation, image acquisition and image processing by ZooImage tools, and PJ Barón
587 contributed with research planning and conceptual guidance, results interpretation and writing
588 of the article. All members participated in the revision and have approved the final article.
589

590 **Acknowledgement**

591

592 We specially thank Dr. Leonardo A. Venerus for his contribution to this study with funds
593 from a grant of Agencia Nacional de Promoción Científica y Tecnológica (ANPCyT PICT
594 2010-2461). Field work was conducted within a UNESCO World Natural Heritage Site and
595 authorized by the “Subsecretaría de Conservación y Areas Protegidas de Chubut”. Partial
596 analyses (i.e., SST and Chl-a) used in this paper were produced with the Giovanni online data
597 system, developed and maintained by the NASA GES DISC (Goddard Earth Sciences Data
598 and Information Services Center). We thank Gabriela N. Williams for her help in obtaining
599 satellite data. Also we thank Ricardo O. Amoroso and Domingo, A. Gagliardini and the
600 Argentina’s National Commission for Space Activities (CONAE) for providing the satellite
601 image used in this paper. Mr. Néstor Ortiz contributed with his expertise in nautical
602 navigation.
603

604 **References**

605 Acha, E.M., Piola, A., Iribarne, O., Mianzan, H., 2015. Ecological Processes at Marine
606 Fronts: Oases in the Ocean. Springer, London, 73 pp.

607 Albaina, A., Irigoien, X., 2004. Relationships between frontal structures and
608 zooplankton communities along a cross-shelf transect in the Bay of Biscay (1995 to 2003).
609 Marine Ecology Progress Series 284, 65-75.
610 Albaina, A., Irigoien, X., 2007. Fine scale zooplankton distribution in the Bay of Biscay
611 in spring 2004. Journal of Plankton Research 29, 851-870.
612 Alcaraz, M., Calbet, A., Estrada, M., Marrasé, C., Saiz, E., Trepat, I., 2007. Physical
613 control of zooplankton communities in the Catalan Sea. Progress in Oceanography 74, 294-
614 312.
615 Alemany, D., Acha, E., Iribarne, O., 2009. The relationship between marine fronts and
616 fish diversity in the Patagonian Shelf Large Marine Ecosystem. Journal of Biogeography 36,
617 2111-2124.
618 Alemany, D., Acha, E.M., Iribarne, O.O., 2014. Marine fronts are important fishing
619 areas for demersal species at the Argentine Sea (Southwest Atlantic Ocean). Journal of Sea
620 Research 87, 56-67.
621 Allan, J.D., 1976. Life history patterns in zooplankton. American Naturalist, 165-180.
622 Amoroso, R.O., Gagliardini, D.A., 2010. Inferring complex hydrographic processes
623 using remote-sensed images: turbulent fluxes in the patagonian gulfs and implications for
624 scallop metapopulation dynamics. Journal of Coastal Research, 320-332.
625 Amoroso, R.O., Parma, A.M., Orensanz, J.L., Gagliardini, D.A., 2011. Zooming the
626 macroscope: medium-resolution remote sensing as a framework for the assessment of a
627 small-scale fishery. ICES Journal of Marine Science: Journal du Conseil 68, 696-706.
628 Bandalos, D.L. and Boehm-Kaufman, M.R., 2009. Four common misconceptions in
629 exploratory factor analysis. In: Lance, C.E and Vandernberg, R.J (Eds.), Statistical and
630 methodological myths and urban legends. Routledge, New York London, pp. 61-87.Basedow,

631 S.L., Tande, K.S., Zhou, M., 2010. Biovolume spectrum theories applied: spatial patterns of
632 trophic levels within a mesozooplankton community at the polar front. Journal of Plankton
633 Research 32, 1105-1119.
634 Belkin, I.M., Cornillon, P.C., Sherman, K., 2009. Fronts in large marine ecosystems.
635 Progress in Oceanography 81, 223-236.
636 Bell, J.L., Hopcroft, R.R., 2008. Assessment of ZooImage as a tool for the classification
637 of zooplankton. Journal of Plankton Research 30, 1351-1367.
638 Benfield, M.C., Grosjean, P., Culverhouse, P.F., Irigoien, X., Sieracki, M.E., Lopez-
639 Urrutia, A., Dam, H.G., Hu, Q., Davis, C.S., Hansen, A., 2007. RAPID: research on automated
640 plankton identification. Oceanography 20, 12-26.
641 Carreto, J.I., Benavides, H.R., Negri, R.M., Glorioso, P.D., 1986. Toxic red-tide in the
642 Argentine Sea. Phytoplankton distribution and survival of the toxic dinoflagellate *Gonyaulax*
643 *excavata* in a frontal area. Journal of Plankton Research 8, 15-28.
644 Conover, W.J., 1999. Statistics of the Kolmogorov-Smirnov type. In: Conover, W.J.
645 (Ed.), Practical nonparametric statistics. John Wiley and Sons, New York, pp. 428-473.
646 Crespi-Abril, A.C., Barón, P.J., 2012. Revision of the population structuring of *Illex*
647 *argentinus* (Castellanos, 1960) and a new interpretation based on modelling the spatio-
648 temporal environmental suitability for spawning and nursery. Fisheries Oceanography 21,
649 199-214.
650 Crespi-Abril, A., Gomila, G.V., Venerus, L., Barón, P.J., 2014. Spatial distribution of
651 cephalopod paralarvae in San José Gulf (Northern Patagonia, Argentina): the role of tidal
652 circulation in larval dispersal. Fisheries Research 152, 13-20.

Derisio, C., Alemany, D., Acha, E.M., Mianzan, H., 2014. Influence of a tidal front on zooplankton abundance, assemblages and life histories in Península Valdés, Argentina. Journal of Marine Systems 139, 475-482.

Dur, G., Hwang, J.S., Souissi, S., Tseng, L.C., Wu, C.H., Hsiao, S.H., Chen, Q.C., 2007. An overview of the influence of hydrodynamics on the spatial and temporal patterns of calanoid copepod communities around Taiwan. Journal of Plankton Research 29, 97-116.

Escribano, R., Hidalgo, P., 2000. Spatial distribution of copepods in the north of the Humboldt Current region o¡ Chile during coastal upwelling. Journal of the Marine Biological Association of the United Kingdom 80, 283-290.

Falkowski, P.G., Oliver, M.J., 2007. Mix and match: how climate selects phytoplankton. Nature Reviews Microbiology, 5, 813-819.

Fernandes, J.A., Irigoien, X., Boyra, G., Lozano, J.A., Inza, I., 2009. Optimizing the number of classes in automated zooplankton classification. Journal of Plankton Research 31, 19-29.

Gagliardini, D.A., Amoroso, R.O., Dell'Arciprete, O.P., Yorio, P., Orensanz, J.M., 2004. Detection of small-scale coastal oceanographic processes through LANDSAT-TM/ETM+ images: implications for the study of biological processes along the Patagonian coasts of Argentina. Gayana (Concepción) 68, 194-200.

Gorsky, G., Ohman, M.D., Picheral, M., Gasparini, S., Stemmann, L., Romagnan, J.-B., Cawood, A., Pesant, S., García-Comas, C., Prejger, F., 2010. Digital zooplankton image analysis using the ZooScan integrated system. Journal of Plankton Research 32, 285-303.

Harris, V., Olhede, S.C., Edwards, M., 2015. Multidecadal spatial reorganisation of plankton communities in the North East Atlantic. Journal of Marine Systems 142, 16-24.

676 Hernández-León, S., Montero, I., 2006. Zooplankton biomass estimated from
677 digitalized images in Antarctic waters: A calibration exercise. Journal of Geophysical
678 Research: Oceans 111, C05S03.
679 Hernández Moresino, R.D., Villanueva Gomila, L., Di Mauro, R., Barón, P.J., 2014.
680 Structural differentiation of the mesozooplankton community in two hydrographic domains of a
681 small basin: the frontal system of San José Gulf (Patagonia, Argentina) as a study case.
682 Journal of Plankton Research 36, 578-584.
683 Hoguane, A. M. (1999). Sea level measurement and analysis in the western Indian
684 Ocean. National report: Mozambique, UNESCO International Oceanographic Commission
685 (IOC), 34 pp.
686 Irigoien, X., Fernandes, J.A., Grosjean, P., Denis, K., Albaina, A., Santos, M., 2009.
687 Spring zooplankton distribution in the Bay of Biscay from 1998 to 2006 in relation with
688 anchovy recruitment. Journal of Plankton Research 31, 1-17.
689 Jennings, S., Greenstreet, S., Hill, L., Piet, G., Pinnegar, J., Warr, K., 2002. Long-term
690 trends in the trophic structure of the North Sea fish community: evidence from stable-isotope
691 analysis, size-spectra and community metrics. Marine Biology 141, 1085-1097.
692 Kerr, S.R., Dickie, L.M., 2001. The biomass spectrum: a predator-prey theory of
693 aquatic production. Columbia University Press, New York, 320 pp.
694 Kiørboe, T., 1993. Turbulence, phytoplankton cell size, and the structure of pelagic
695 food webs. Advances in Marine Biology 29, 1-72.
696 Kiørboe, T., 2008. A mechanistic approach to plankton ecology. Princeton University
697 Press, Princeton, 209 pp.

Krupica, K.L., Sprules, W.G., Herman, A.W., 2012. The utility of body size indices derived from optical plankton counter data for the characterization of marine zooplankton assemblages. Continental Shelf Research 36, 29-40.

Largier, J.L., 1993. Estuarine fronts: How important are they? Estuaries 16, 1-11.

Lavaniegos, B., Molina-González, O., Murcia-Riaño, M., 2015. Zooplankton functional groups from the California Current and climate variability during 1997-2013. Cicimar Oceánides 30, 45-62.

Le Fevre, J., 1986. Aspects of the biology of frontal systems. Advances in Marine Biology 23, 163-299.

Lehette, P., Hernández-León, S., 2009. Zooplankton biomass estimation from digitized images: a comparison between subtropical and Antarctic organisms. Limnology and Oceanography: Methods 7, 304-308.

Lewis, M.R., 2002. Variability of plankton and plankton processes on the mesoscale. In: Williams, P.J., Le, B., Thomas, D.N., Reynolds, C.S. (Eds.), Phytoplankton Productivity: Carbon Assimilation in Marine and Freshwater Ecosystems. Blackwell, London, pp. 141–155.

MacKenzie, B.R., 2002. Understanding the role of turbulence on fisheries production during the first century of ICES. ICES Marine Science Symposia 215, 227-236.

Mann, K.H., Lazier, J.R.N., 1991. Dynamics of marine ecosystems: Biological-physical interactions in the oceans. Blackwell Scientific Publications, Boston, 466 pp.

Manríquez, K., Escribano, R., Hidalgo, P., 2009. The influence of coastal upwelling on the mesozooplankton community structure in the coastal zone off Central/Southern Chile as assessed by automated image analysis. Journal of Plankton Research 31, 1075-1088.

Marcolin, C.R., Gaeta, S., Lopes, R.M., 2015. Seasonal and interannual variability of zooplankton vertical distribution and biomass size spectra off Ubatuba, Brazil. Journal of Plankton Research 37, 808-819.

Mauna, A.C., Franco, B.C., Baldoni, A., Acha, E.M., Lasta, M.L., Iribarne, O.O., 2008. Cross-front variations in adult abundance and recruitment of Patagonian scallop (*Zygochlamys patagonica*) at the SW Atlantic shelf break front. ICES Journal of Marine Science: Journal du Conseil 65, 1184-1190.

Moreira, D., Simionato, C., Dragani, W., 2011. Modeling ocean tides and their energetics in the North Patagonia Gulfs of Argentina. Journal of Coastal Research 27, 87-102.

Pisoni, J.P., Rivas, A.L., Piola, A.R., 2015. On the variability of tidal fronts on a macrotidal continental shelf, Northern Patagonia, Argentina. Deep Sea Research Part II: Topical Studies in Oceanography 119, 61-68.

Platt, T., Denman, K., 1977. Organization in the pelagic ecosystem. Helgoländer wissenschaftliche Meeresuntersuchungen 30, 575-581.

Platt, T., Harrison, W.G., 1985. Biogenic fluxes of carbon and oxygen in the ocean. Nature 318, 55-58.

Punchi-Manage, R., Getzin, S., Wiegand, T., Kanagaraj, R., Savitri Gunatilleke, C., Nimal Gunatilleke, I., Wiegand, K., Huth, A., 2013. Effects of topography on structuring local species assemblages in a Sri Lankan mixed dipterocarp forest. Journal of Ecology 101, 149-160.

Quinones, R.A., Platt, T., Rodríguez, J., 2003. Patterns of biomass-size spectra from oligotrophic waters of the Northwest Atlantic. Progress in Oceanography 57, 405-427.

743 Ramírez, F., 1996. Composición, abundancia y variación estacional del zooplankton de
744 red del Golfo San Matías [Composition, abundance and seasonal variation of net zooplankton
745 of San Matías Gulf]. Frente Marítimo 16, 157-167.
746 Rivas, A., 1990. Heat-balance and annual variation of mean temperature in the north-
747 patagonian gulfs. Oceanologica Acta 13, 265-272.
748 Sabatini, M., Martos, P., 2002. Mesozooplankton features in a frontal area off northern
749 Patagonia (Argentina) during spring 1995 and 1998. Scientia Marina 66, 215-232.
750 Sheldon, R., Prakash, A., Sutcliffe, W., 1972. The size distribution of particles in the
751 ocean. Limnology and Oceanography 17, 327-340.
752 Shin, Y.J., Rochet, M.-J., Jennings, S., Field, J.G., Gislason, H., 2005. Using size-
753 based indicators to evaluate the ecosystem effects of fishing. ICES Journal of Marine
754 Science: Journal du Conseil 62, 3.
755 SHN (Servicio de Hidrografía Naval), 2000. Derrotero Argentino Parte II. Costa del
756 Atlántico. Desde Cabo San Antonio a Cabo Vírgenes y Punta Dungeness y Suplemento. 9th
757 edition. Buenos Aires, Argentina: Servicio de Hidrografía Naval, Armada de la República
758 Argentina, Publicación H 202.
759 SHN (Servicio de Hidrografía Naval), 2008. Tablas de Marea. Buenos Aires, Argentina:
760 Servicio de Hidrografía Naval, Ministerio de Defensa, Publicación H 610.
761 Smayda, T.J., 1970. The suspension and sinking of phytoplankton in the sea.
762 Oceanography and Marine Biology. An Annual Review 8, 353-414.
763 Spinelli, M.L., Pájaro, M., Martos, P., Esnal, G.B., Sabatini, M., Capitanio, F.L., 2011.
764 Potential zooplankton preys (Copepoda and Appendicularia) for *Engraulis anchoita* in relation
765 to early larval and spawning distributions in the Patagonian frontal system (SW Atlantic
766 Ocean). Scientia Marina 76, 39-47.

Sprules, W.G., Munawar, M., 1986. Plankton size spectra in relation to ecosystem productivity, size, and perturbation. Canadian Journal of Fisheries and Aquatic Sciences 43, 1789-1794.

Vandromme, P., Stemmann, L., Garcìa-Comas, C., Berline, L., Sun, X., Gorsky, G., 2012. Assessing biases in computing size spectra of automatically classified zooplankton from imaging systems: A case study with the ZooScan integrated system. Methods in Oceanography 1, 3-21.

Vandromme, P., Nogueira, E., Huret, M., Lopez-Urrutia, A., González-Nuevo González, G., Sourisseau, M., Petitgas, P., 2014. Springtime zooplankton size structure over the continental shelf of the Bay of Biscay. Ocean Science 10, 821-835.

Viñas, M.D., Negri, R.M., Cepeda, G.D., Hernández, D., Silva, R., Daponte, M.C., Capitanio, F.L., 2013. Seasonal succession of zooplankton in coastal waters of the Argentine Sea (Southwest Atlantic Ocean): prevalence of classical or microbial food webs. Marine Biology Research 9, 371-382.

Viñas, M.D., Ramírez, F.C., Santos, B.A., Marrari, M., 2007. Spatial and temporal distribution patterns of Cladocera in the Argentine Sea. Hydrobiologia 594, 59-68.

Zhou, M., 2006. What determines the slope of a plankton biomass spectrum? Journal of Plankton Research 28, 437-448.

Zhou, M., Tande, K.S., Zhu, Y., Basedow, S., 2009. Productivity, trophic levels and size spectra of zooplankton in northern Norwegian shelf regions. Deep-Sea Research Part II: Tropical Studies in Oceanography 56, 1934-1944.

**Highlights:**

- SST and Chl-a confirm two hydrographic domains in San José Gulf in spring-summer.
- Contrasting hydrographic conditions affect the mesozooplankton community structure.
- Size spectra could reflect distinct trophic pathways in two clusters of stations.
- A late-summer peak of biomass occurred only in the stratified domain.
- Intermediate hydrodynamic conditions may lead to community transitional zone.